ACS APPLIED MATERIALS & INTERFACES

www.acsami.org

Research Article

Effect of Sodium Phosphate Coating on Cu and Mg-Substituted P2−$Na_{0.67}Ni_{0.33}Mn_{0.67}O_2$ for Improving the Cycling Performance of Sodium-Ion Capacitors

Song Yeul Lee, Yang Soo Kim, Sangho Park, Yun-Sung Lee,* and Yong Il Park*

Cite This: *ACS Appl. Mater. Interfaces* 2023, 15, 54530−54538

Read Online

ACCESS | Metrics & More | Article Recommendations | Supporting Information

ABSTRACT: Sodium-ion capacitors (SICs) bridge the performance gaps between batteries and supercapacitors by providing a high energy and power density in a single configuration. As battery-type active materials, sodium preintercalated layered metal oxides are desirable owing to their unique crystal structure, simple synthesis process, and high working voltage. However, their poor cyclic stability and low kinetics limit their application. Herein, we report increased rate capability and cycle stability achieved by introducing transition metal substitution and surface coating strategies. By substituting a portion of Ni and Mn with Cu and Mg (the sample name was denoted as NMCM), the P2−O2 transition which occurs at high voltages was alleviated. Additionally, a thin and uniform sodium phosphate coating layer suppressed surface side reactions occurring during charge−discharge processes, as observed through ex-situ X-ray photoelectron spectroscopy and ex-situ transmission electron microscopy. Compared to the pristine sample, the capacity improved by 48% at a high current density of 4 A g^{-1}. After 100 cycles, the sodium-phosphate-coated sample (NMCM@P) retained about 90% of its capacity, whereas NMCM had a capacity retention of 63%. When evaluating the longer stability of SIC full cells, NMCM@P exhibited an outstanding stability of 71% after 5000 cycles. This was higher than that of NMCM, which retained only 17% of its initial capacity.

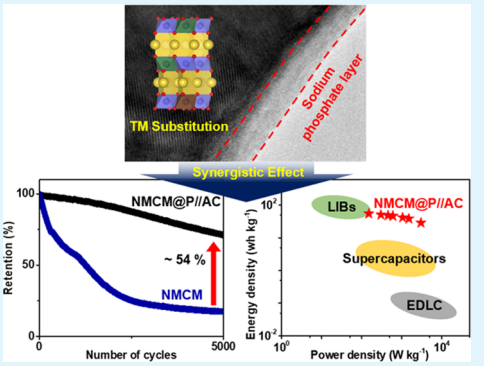

KEYWORDS: *sodium, capacitor, energy storage, battery-type cathode, hybrid capacitor*

INTRODUCTION

As the climate crisis worsens, renewable energy development is becoming more crucial. To efficiently utilize intermittent renewable energy, it has become essential to develop large-scale energy storage techniques that store the produced energy.[1−3] Although lithium-ion batteries currently dominate the market, the continuous increase in their price has led to research into the development of next-generation energy storage technologies.[4−6] Sodium-ion batteries (SIBs) are considered promising candidates for large-scale energy storage owing to their abundance and relatively low prices.[7,8] Additionally, solvated Na ions are smaller than solvated Li-ions, resulting in lower viscosity and higher ionic conductivity, thereby exhibiting a faster kinetic performance. However, the low power density and poor cyclic lifespan of SIBs still limit their utilization. Supercapacitors, on the other hand, have excellent cycle stability and high power density but low energy capacity.[9,10] Sodium-ion capacitors (SICs), which can have high energy and power density, are gaining attention as a potential solution to this trade-off between energy capacity and power density.[11−13] SICs consist of a battery-type electrode with high energy capacity and a capacitor-type electrode with high power density.[14] Since the two electrodes have different kinetic properties, the SIC design needs to be optimized. Material selection and surface modification are essential for improving the relatively sluggish kinetic properties and poor cyclic lifespan of the battery-type electrode.

Among various SIB cathode materials, many studies have been conducted on layered oxides because of their easy synthesis, relatively low price, and good electrochemical performance.[15,16] Layered oxides, such as $NaMO_2$ (M = transition metal), are generally categorized as the O3 or P2-type depending on whether sodium ions occupy the octahedral site or the prismatic site. Depending on the order in which oxygen is stacked, ABCABC is classified as O3-type and ABBA as P2-type. The O3 structure exhibits complex phase changes during charging and discharging by the Na ion hopping process, whereas the P2 structure is structurally more stable owing to the direct diffusion of Na ions. Na−Ni−Mn-O (NM) materials have been studied considerably because of the

Received: September 6, 2023
Revised: November 1, 2023
Accepted: November 1, 2023
Published: November 15, 2023

https://doi.org/10.1021/acsami.3c13351
ACS Appl. Mater. Interfaces 2023, 15, 54530−54538

relatively low price of manganese, high theoretical capacity, and high redox potential of nickel (above 3 V).[17,18] However, the P2−O2 transition, which occurs above 4.1 V, limits the cutoff voltage of the material and causes capacity fade and poor cyclic stability. Substitution with inert cations can be an effective strategy to overcome this limitation by improving the structural stability and suppressing the Jahn−Teller distortion and Na^+/vacancy ordering. Singh et al. and Hou et al.[19,20] reported the electrochemical performance after replacing Ni ions with Mg ions in the Na−Ni−Mn-O structure. The substitution of Ni ions with Mg ions inhibits the P2−O2 phase transition by stabilizing the reversible OP4 phase during the charging process and also increases the lattice parameters and the *d*-spacing of the diffusion layer to improve cycle stability and rate performance. Additionally, it has been reported that the substitution of cations with copper increases the average discharge voltage while improving structural stability.[21] Also, copper has the advantage of being an abundant and inexpensive element on earth.

Surface coating is another promising approach for improving the cyclic stability. A thin Al_2O_3 layer was introduced on the surface of P2-type $Na_{2/3}Ni_{1/3}Mn_{2/3}O_2$ by wet chemistry or atomic layer deposition (ALD).[22] The Al_2O_3 layer suppresses side reactions that occur during charging and discharging, minimizing the generation of byproducts and the exfoliation of active materials. Ramasamy et al. introduced a MgO layer by solution-free melt impregnation on the surface of P2-type $Na_{0.5}Ni_{0.26}Cu_{0.07}Mn_{0.67}O_2$ (NCM).[23] They demonstrated that MgO-modified NCM improves the rate performance at high current densities because the MgO layer stabilizes the solid electrolyte interface (SEI) layer and prevents the dissolution of metal ions. Additionally, surface modification with sodium phosphate ($NaPO_3$) has several advantages.[24] First, abundant phosphorus resources have the advantage of relatively low prices. Also, the $NaPO_3$ layer was easily formed via reaction with the residual sodium source on the surface of the active material. This layer has a high Na^+ ionic conductivity, which is favorable for Na^+ diffusion. In this study, we introduce two substitution and surface coating techniques to enhance the rate performance and cycle stability of the SIB cathode and fabricate SICs. Also, we analyze the surface of the electrode after cycling with ex-situ X-ray photoelectron spectroscopy (XPS) and ex-situ transmission electron microscopy (TEM) to investigate the effect of the passive layer.

EXPERIMENTAL SECTION

P2-Type Na−Ni−Mg−Cu−Mn-O Synthesis and Sodium Phosphate Coating. P2-type NM and Na−Ni−Mg−Cu−Mn-O (NMCM) were synthesized by using coprecipitation. Sulfate compounds of nickel, magnesium, copper, and manganese were dissolved in distilled water in a molar ratio of 0.15:0.1:0.05:0.7 (Solution 1). Distilled water was used to dissolve the same quantity of sodium carbonate as the total amount of metals, and ammonium hydroxide was added to induce precipitation (Solution 2). Both solutions were dropped into the reaction flask while being stirred before the reaction at 60 °C for 24 h. The product was filtered and washed several times with distilled water. The product powder dried at 100 °C overnight was calcined at 500 °C for 5 h to prepare multimetal oxide. The synthesized metal oxide was mixed with sodium carbonate in a molar ratio of 2:1, and the mixture was heated to 900 °C and maintained in an airy atmosphere for 24 h to synthesize P2-type NMCM. For comparison of electrochemical performance, single-element substitution samples of Mn (denoted as NMM) and Cu (denoted as NMC) were prepared using the same procedure. To coat NMCM with sodium phosphate, ammonium phosphate was added to as much as 10 wt % of the NMCM sample. The mixture was heated to 190 °C and maintained for 1 h before being heated to 300 °C and maintained for 4 h.

Characterizations. The Na, Mn, Ni, Mg, and Cu contents of the final product were measured using inductively coupled plasma optical emission spectrometry (ICP−OES, Optima 8300). The coated surface of the electrode was analyzed using a time-of-flight secondary ion mass spectrometer (ToF−SIMS, ION-TOF GmbH, Münster, Germany) with a pulsed 30 keV Bi^+ primary beam and Fourier-transform infrared (FT-IR) spectroscopy (Spectrum 400, PerkinElmer). The structure of the material was characterized using X-ray diffraction (XRD, Panalytical) in the range 10−100° under step scanning mode with 45 kV/40 mA, 0.007°/step, and 198 s/step exposure time. Rietveld refinement of the collected data was performed by using the Topas5 (Bruker Inc.) code. The morphology of the material was observed by using scanning electron microscopy (SEM, Hitachi SU-70, Japan) and TEM (TECNAI G2 F20), and the distribution of each element in the material was confirmed by energy dispersive X-ray spectroscopy (EDS) elemental mapping. The surface state of the electrode after cycling was analyzed using XPS (K-ALPHA$^+$). The electrode was disassembled in a glovebox and rinsed several times with dimethyl carbonate (DMC).

Electrochemical Measurements. The electrode was prepared by mixing the active material, carbon black, and poly(vinylidene fluoride) (PVDF) with *N*-methylpyrrolidinone (NMP) in a weight ratio of 8:1:1. The slurry was cast on an Al foil and kept in a vacuum oven at 120 °C overnight. The average active material loading of the electrode was 1.6 mg cm^{-2}. Electrochemical measurements of all samples were evaluated by assembling 2032-coin cells. Half cells were prepared by using sodium metal as a counter electrode and a reference electrode. Whatman glass fiber was used as the separator, and 1 M $NaClO_4$ mixed with ethylene carbonate and dimethyl carbonate (EC:DMC, 1:1 volume ratio) was used as the electrolyte.

Cyclic voltammetry (CV) and electrochemical impedance spectroscopy (EIS) were performed using a potentiostat (Bio-Logic electrochemical workstation, SP-150, France) at room temperature at a potential window of 1.5−4.3 V, and EIS results were fitted using ZMAN software. The galvanostatic charge−discharge and cyclic performance results were collected by using a Won-A-Tech battery tester (WBCS 3000, Korea). The SIC was prepared using activated carbon (AC) as the capacitor-type anode, and the ratio of the negative electrode to the positive electrode (N/P ratio) was evaluated as 1:1, 1:2, and 1:3 weight ratios. Electrochemical measurements of the SIC were performed in the 0.01−3.0 V range using the same equipment as the half-cell. The specific energy (E, Wh kg^{-1}) and power (P, W kg^{-1}) of the SIC were calculated using the following equations

$$\text{Energy density}(E, \text{Wh kg}^{-1}) = \int_{t_1}^{t_2} IV\,\mathrm{d}t \tag{1}$$

$$\text{Power density}(P, \text{W kg}^{-1}) = \frac{E}{t} \tag{2}$$

where t_1 (s) and t_2 (s) represent the start and end times of cell discharge, V (V) is the working potential, I (A g^{-1}) is the discharge current density, and t (s) is the discharge time.

RESULTS AND DISCUSSION

NM and NMCM were synthesized by using a solid-state reaction of transition metal oxides with sodium carbonate. The transition metal oxides were prepared using the coprecipitation method. Each transition metal precursor was dissolved in a specific ratio and added to an ammonia solution. The precipitate was converted to multitransition metal oxides by heat treatment. The molar ratio of each element in the synthesized NMCM was calculated using the ICP−OES results and the formula is $Na_{0.60}Ni_{0.17}Mg_{0.11}Cu_{0.06}Mn_{O.66}O_2$ (Table S1).

https://doi.org/10.1021/acsami.3c13351
ACS Appl. Mater. Interfaces 2023, 15, 54530−54538

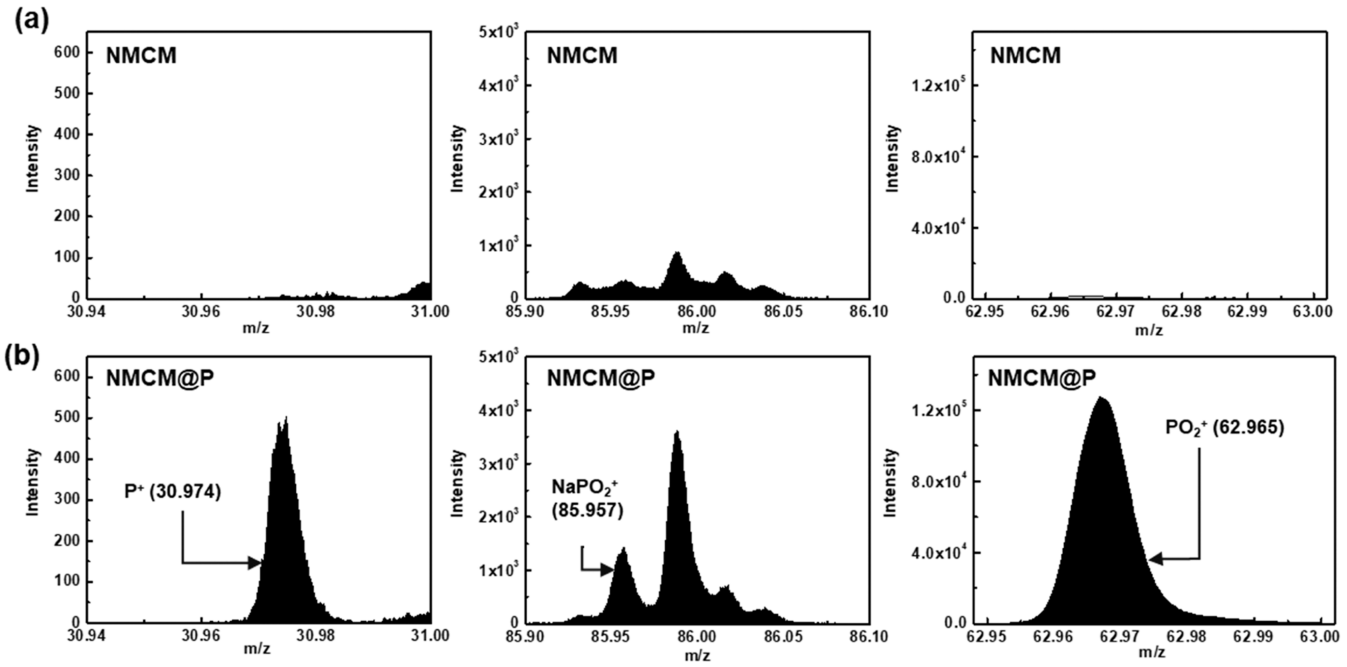

Figure 1. ToF−SIMS spectra of (a) NMCM and (b) NMCM@P.

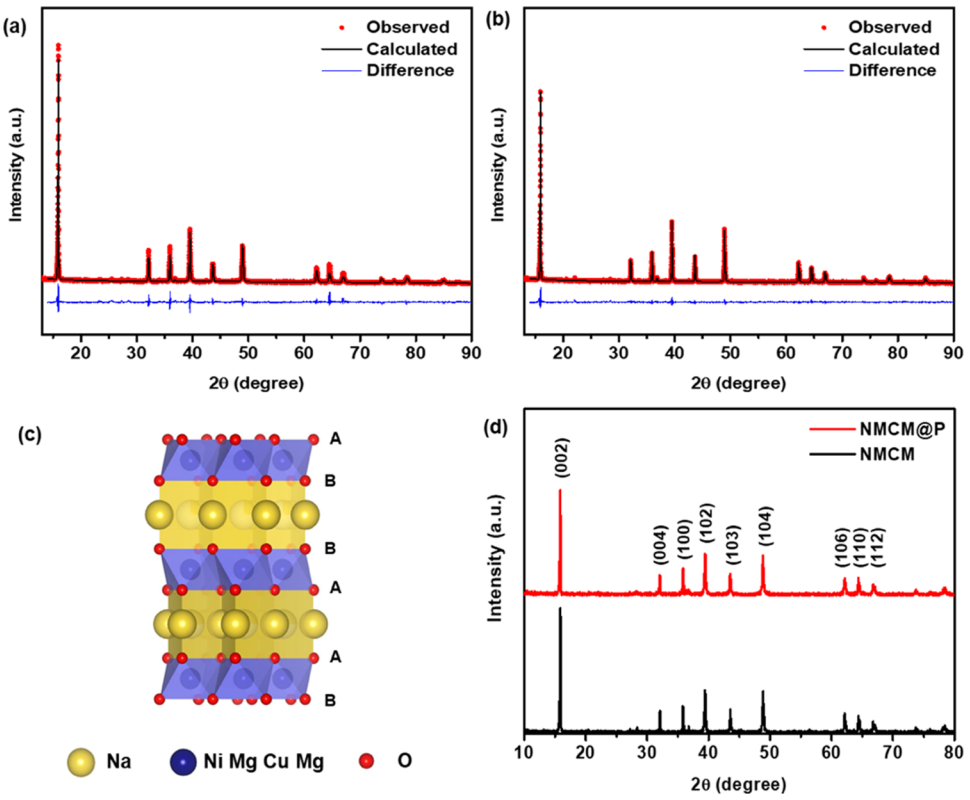

Figure 2. XRD patterns of (a) NM and (b) NMCM after refinement. (c) Illustration of NMCM crystal structure. (d) XRD patterns of NMCM and NMCM@P.

The coating layer was formed by the reaction between a phosphate source and a sodium source (such as Na_2O or Na_2CO_3) that was still on the NMCM surface. $NH_4H_2PO_4$ changed to H_3PO_4 at 190 °C and covered the NMCM surface. At 300 °C, it reacted with surface residues to form sodium phosphate.[25] In the ToF−SIMS spectra, no peaks of the P^+ (m = 30.97), $NaPO^{2+}$ (m = 85.96), and PO^{2+} (m = 62.97) fragments of sodium phosphate were detected in the as-synthesized NMCM (Figure 1a). After coating, however, peaks of sodium phosphate fragments were detected (Figure 1b), demonstrating the successful formation of the sodium phosphate layer on the NMCM surface. Additionally, fragments of $Na_3PO_4^+$ and $Na_2P_2O_7^+$ exhibited strong intensity after coating (Figure S1). However, these results make it

https://doi.org/10.1021/acsami.3c13351
ACS Appl. Mater. Interfaces 2023, 15, 54530−54538

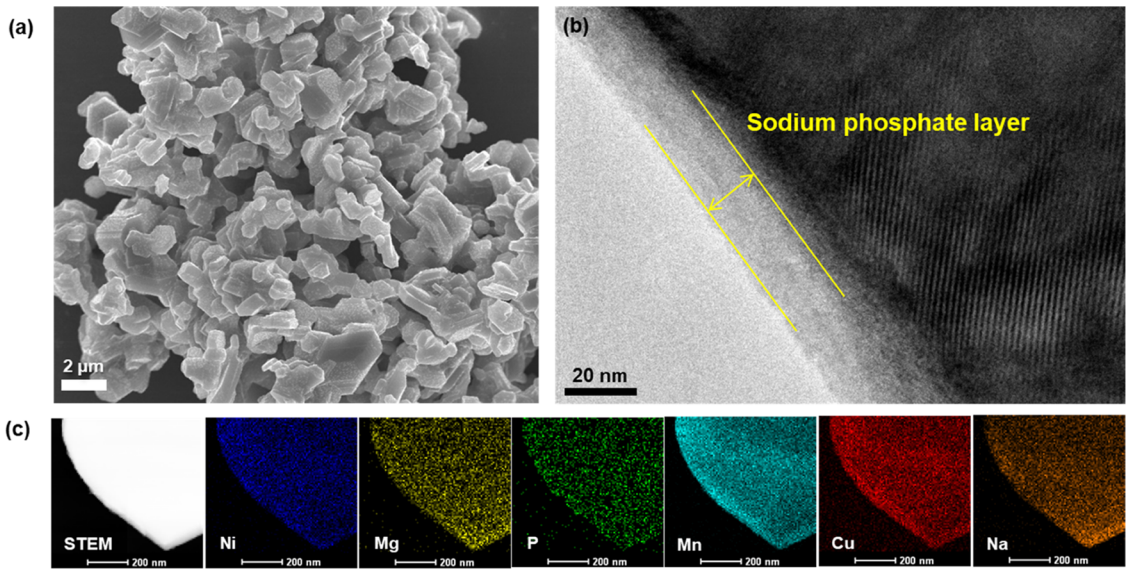

Figure 3. (a) SEM image of NMCM@P. (b) TEM image of NMCM@P. (c) STEM image of NMCM@P and its element mapping.

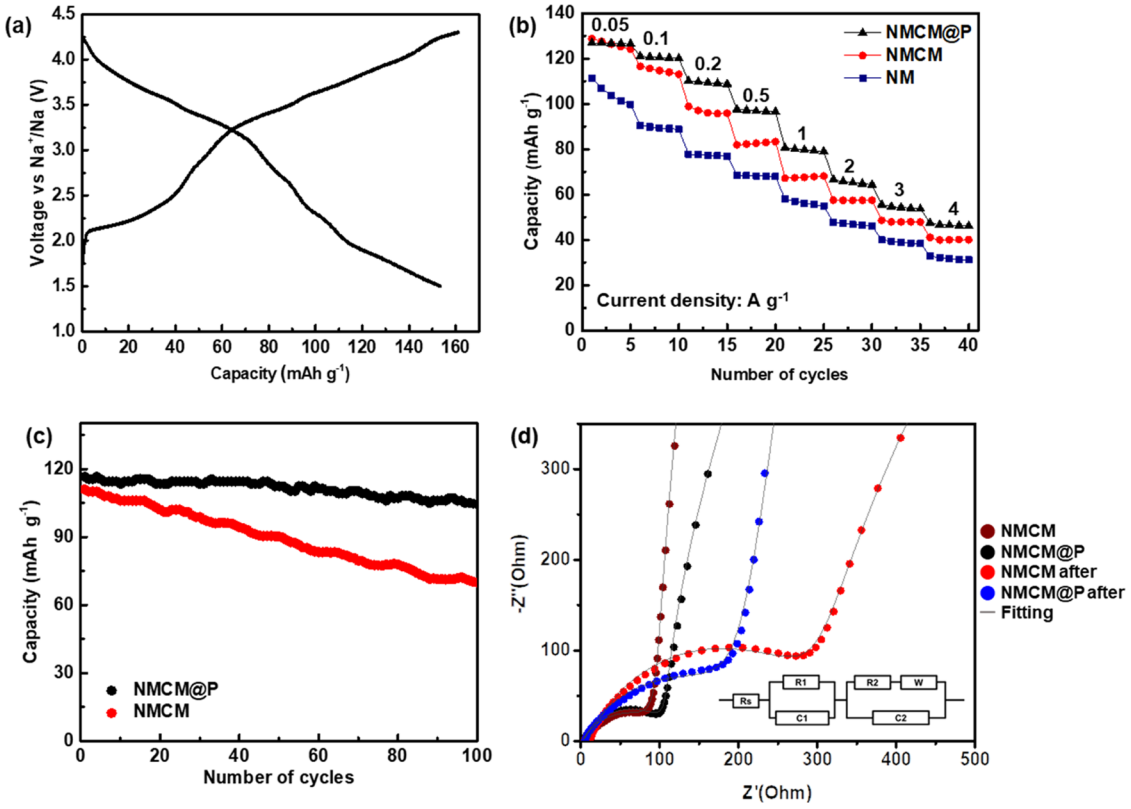

Figure 4. (a) Galvanostatic charge−discharge voltage profiles of NMCM@P at 20 mA g^{-1}. (b) Rate capability of NM, NMCM, and NMCM@P. (c) Cyclic performance of NMCM and NMCM@P at 100 mA g^{-1}. (d) Nyquist plot of NMCM and NMCM@P.

difficult to distinguish materials with similar compositions such as $(NaPO_3)_n$, Na_2PO_4H, and Na_3PO_4. To further analyze the composition of the coated layer on the surface, FT-IR and Raman spectroscopy were conducted. As shown in Figure S2a, the FT-IR spectrum revealed various peaks attributed to phosphate after coating, including a distinct peak corresponding to P−O−P emerging at 925 cm^{-1}. Moreover, the XPS spectrum in Figure S2b demonstrated the presence of a previously reported sodium polyphosphate complex, $(NaPO_3)_n$, at approximately 132.6 eV, rather than Na_3PO_4 at 136 eV. Consequently, we concluded that the surface layer is a composite containing both $(NaPO_3)_n$ and Na_3PO_4, rather than a single component.[26]

The XRD Rietveld refinement patterns of NM and NMCM are shown in Figure 2a,2b. Each peak is indexed into a P2-type layered structure with an $P6_3/mmc$ space group. Although the two kinds of ions were substituted, impurity peaks did not appear, indicating that no impurities were generated during the synthesis process and the Mg and Cu ions were well substituted at the Ni position. The illustration in Figure 2c

https://doi.org/10.1021/acsami.3c13351
ACS Appl. Mater. Interfaces 2023, 15, 54530−54538

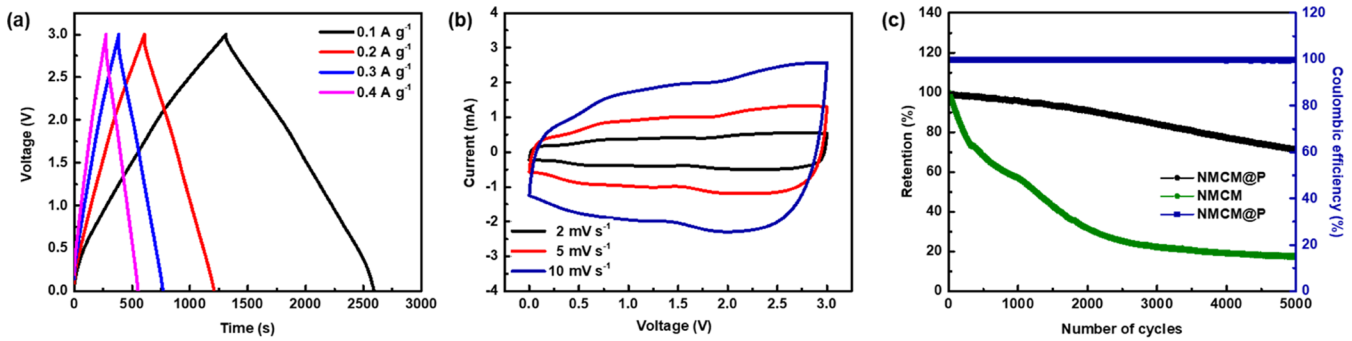

Figure 5. (a) Galvanostatic charge−discharge voltage profiles of NMCM@P//AC. (b) Cyclic voltammetry curves of NMCM@P//AC. (c) Cyclic performance and Coulombic efficiency at 0.7 A g^{-1}.

exhibited the crystal structure of NMCM. Sodium-ions occupied two prismatic sites, which are in face-sharing site with TMO_6 (TM = transition metal, e.g., Mn, Ni, Cu, Mg) and edge-sharing between TMO_6 octahedra.[27] The cell volume was increased owing to cation substitution because the radii of Mg^{2+} (0.72 Å) and Cu^{2+} (0.73 Å) ions are larger than that of Ni^{2+} (0.69 Å) ions (Table S2). After sodium phosphate coating, no peaks from the coating layer were detected because the layer was thinly coated on the NMCM surface (Figure 2d).

The microstructures of the NMCM and NMCM@P samples are shown in Figures S3 and 3a. NMCM had a platelike shape with an average size of 3−5 μm. For NMCM@P, aggregation occurred between particles but there was no significant change in the morphology after coating. The TEM image shows the formation of a thin and uniform sodium phosphate layer with a thickness of 15 nm on the surface of the NMCM (Figure 3b). The EDS elemental mapping shows that the substituted cations were well dispersed in the particle and phosphorus was evenly distributed on the surface of the particle (Figure 3c). To assess the stability of the sodium phosphate layer, we kept the NMCM@P under air condition for 2 weeks. Subsequent analyses were conducted to confirm the stability of the surface layer. As shown in Figure S4, the surface layer remained stable even after being exposed to air for 2 weeks. Additionally, the FT-IR analysis results revealed that the spectra for the fresh sample and the sample after 2 weeks were similar, with no appearance of additional impurity peaks (Figure S5).

The electrochemical performance of each sample was evaluated with a half-cell assembled with Na metal as the counter and reference electrodes. In the CV curves, the peak pairs below 3 V are associated with the Mn^{3+}/Mn^{4+} redox reaction, while those above 3 V are associated with the Ni^{2+}/Ni^{4+} redox reaction (Figure S6). Galvanostatic charge and discharge (GCD) curves of NM and NMCM are shown in Figure S7. Several voltage plateaus appeared in the charge−discharge curves of the NM sample, indicating redox reactions of transition metals. The plateau around 4 V is caused by the P2−O2 phase transition of the Na−Ni−Mn-O materials and the glide and expansion of the transition metal layers.[28] The plateaus between 3 and 3.9 V and below 2 V are associated with the redox reaction of Ni ion and Mn ion due to Na intercalation/deintercalation. It is worth noting that Mg and Cu substitution caused the structure to be stable and plateaus above 3 V to be smooth in the GCD curve of the NMCM sample. Additionally, after sodium phosphate coating, there was no change in the NMCM GCD profile (such as an extra plateau and overpotential) (Figure 4a). Figures 4b and S8a show the rate performance of each sample. NMCM@P exhibited specific capacities of 127, 121, 110, 98, 81, 67, 56, and 48 mAh g^{-1} at current densities of 0.05, 0.1, 0.2, 0.5, 1, 2, 3, and 4 A g^{-1}, respectively. NMCM@P showed better rate capabilities than NM, NMM, NMC, and NMCM, and a detailed analysis will be discussed later. The capacity retention of each sample was evaluated at a current density of 0.1 A g^{-1} (Figures 4c and S8b). After 100 cycles, NMCM retained about 63% of its initial capacity, whereas NMCM@P retained about 90% of its initial capacity. The resistances of NMCM and NMCM@P can be compared using the EIS analysis results before and after the cycle (Figure 4d). Rs represents the ohmic resistance in the high-frequency region, including the resistance of the electrolyte and the contact resistance of the material. In the high to midfrequency range, $R1$ and $C1$ stand for the resistance and capacitance of ion transfer within the SEI film, respectively. The subsequent semicircle in the middle-frequency spectrum is related to the charge transfer resistance ($R2$) and the capacitance of the double layer ($C2$). Finally, the Warburg impedance (W), which is associated with the diffusion of sodium ions, is depicted as a sloping line in the low-frequency range. Comparing the resistance caused by the SEI layer before and after the cycling, the resistance for NMCM@P increased from 98 to 200 Ω, while for the pristine NMCM, it increased more significantly from 112 to 290 Ω. This increase is thought to be due to the suppressive effect of the sodium phosphate layer on the formation of the SEI layer. The resistance difference is discussed more in-depth using full cells. Consequently, the synergic effect of Mg and Cu substitution and the sodium phosphate layer could improve the electrochemical performances of NMCM@P.

SIC full cells were assembled by using NMCM and NMCM@P as a cathode and AC as an anode. The half-cell performance of AC was measured with same electrolyte in the range of 0.01−2.7 V and is shown in Figure S9. To balance the capacity of the anode and cathode, the GCD of the SICs was measured at various weight ratios of the anode and cathode materials, and SICs with a weight ratio of 1:1 showed better rate capability than those with other weight ratios (Figures 5a and S10). As shown in Figures 5b and S11, the shape of the CV curves was almost rectangular, indicating an energy storage mechanism corresponding to the nonfaradaic capacitive reaction and faradaic sodium-ion intercalation/deintercalation reaction. The performance improvement with a sodium phosphate coating was prominent in long-term cyclic stability measurements (Figures 5c and S12). After 5000 cycles at 0.7 A g^{-1}, NMCM had only a 17% retention, whereas the NMCM@P, which used a 10% weight ratio of ammonium phosphate,

https://doi.org/10.1021/acsami.3c13351
ACS Appl. Mater. Interfaces 2023, 15, 54530−54538

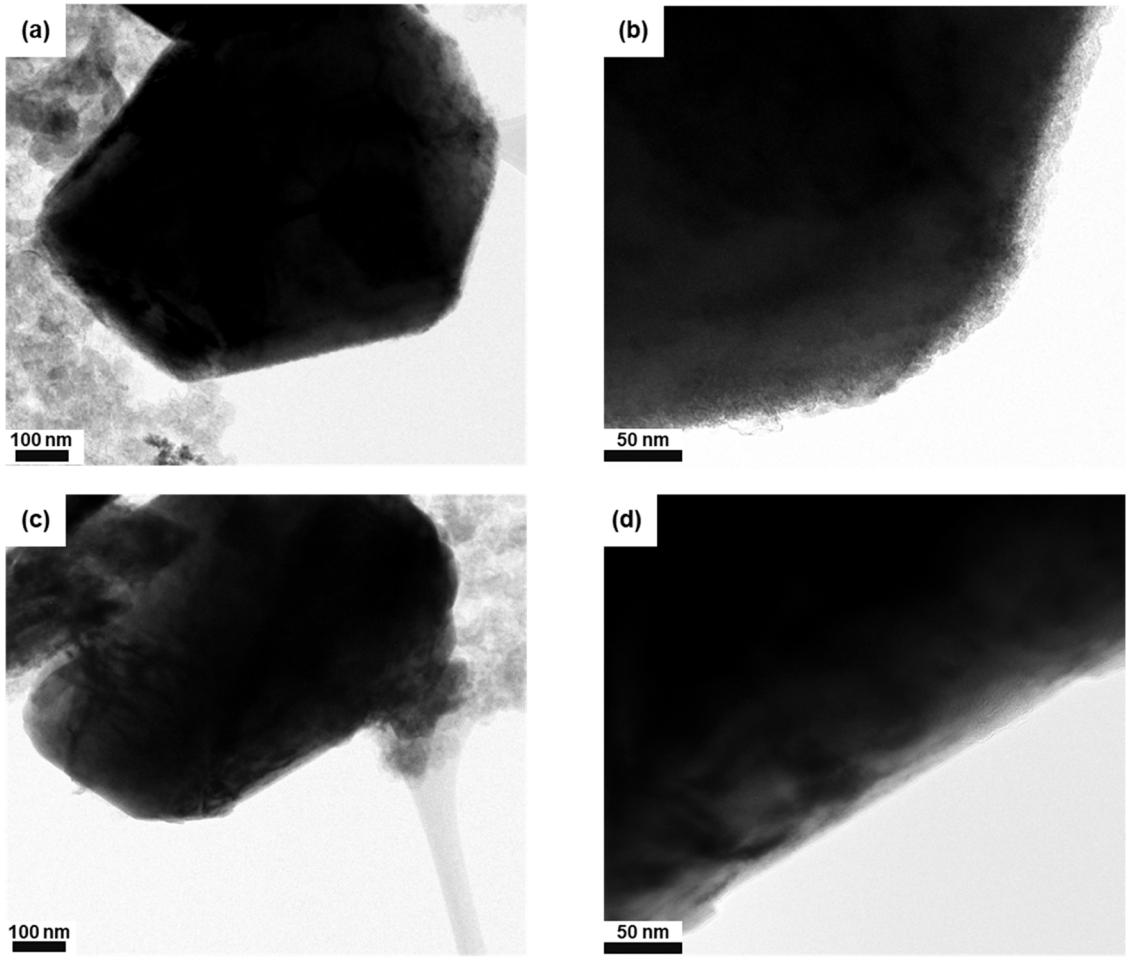

Figure 6. TEM images of NMCM (a, b) and NMCM@P (c, d) after 5000 cycles.

showed an excellent stability of approximately 71 with 99.5% Coulombic efficiency.

To understand the reasons for the improvement in long-term cycle stability, we analyzed the properties of the electrode materials before and after cycling. After cycling, the surface morphologies of the NMCM and NMCM@P electrodes were observed by TEM (Figure 6). The surface of NMCM was damaged, and insulating byproducts such as Na_2CO_3, $RNaCO_3$, and Na_2O were formed on the surface. Compared with bare NMCM, the coated NMCM@P had a smooth interface without apparent damage and byproducts on the surface, meaning that the sodium phosphate layer could protect the surface of the active materials and inhibit the byproduct formation. To identify components of CEI layer, ex-situ XPS analysis of the electrode surface was conducted after cycling. As shown in Figure 7a,b, the carbon and oxygen spectra can be deconvoluted into several peaks. The two peaks at 284.6 and 283.15 eV shown in the C 1s spectrum correspond to C−C and C−H bonds, respectively. Furthermore, the peak at 529.6 eV in the O 1s spectrum is attributed to the M-O peak, indicating the presence of metal oxides. Notably, the peaks at 287.95 and 286.10 eV observed in the C 1s spectrum are associated with C═O and C−O bonds, respectively. These correspond to the peaks at 531.15 and 534.20 eV in the O 1s spectrum, suggesting the presence of CEI components such as Na_2CO_3, $RNaCO_3$, and Na_2O.[29,30] These byproducts produced on the surface of the active material significantly impact the resistance of the material. This can be confirmed using EIS analysis. The Nyquist plots of each sample before and after cycling are shown in Figure 7c,7d. The charge transfer resistance before the cycle was smaller in NMCM@P than in NMCM, and the difference in the resistance became more prominent after the cycle.

The energy and power densities of the SIC using NMCM@P were calculated based on the GCD result and the total mass of the cathode and anode electrodes. NMCM@P//AC showed a maximum energy density of 55 Wh kg^{-1} and a maximum power density of 3000 W kg^{-1}. This electrochemical performance is compared in the Ragone plot (Figure 8). NMCM@P//AC had not only higher energy density and power density compared to other SICs and LICs using battery-type cathode, including P2−$Na_{0.67}Co_{0.5}Mn_{0.5}O_2$//ZIF-8,[31] $Na_{0.4}MnO_2$//AC,[32] $LiNi_{1.5}Mn_{1.5}O_4$//AC,[33] $LiMn_2O_4$//AC,[34] and MCM//AC,[35] but also showed results comparable to those achieved using battery-type anodes.[36−39] As shown in Figure 8b, the NMCM@P//AC SICs demonstrate a performance intermediate between a battery and a capacitor, serving as a potential candidate to bridge the gap between these two distinct devices.

CONCLUSIONS

In summary, we combined two strategies—substitution with Mg and Cu and surface coating with sodium phosphate, to enhance the rate performance and cycle stability of NM. Mg

https://doi.org/10.1021/acsami.3c13351
ACS Appl. Mater. Interfaces 2023, 15, 54530−54538

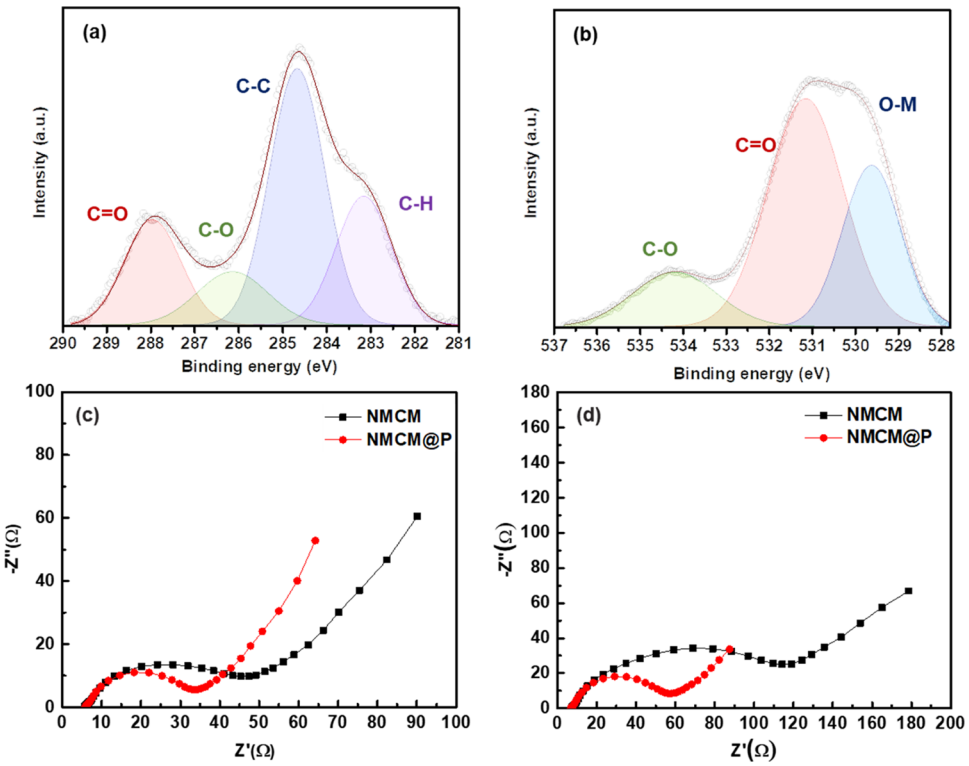

Figure 7. XPS spectra of NMCM after cycles: (a) C 1s and (b) O 1s. Nyquist plot of NMCM and NMCM@P (c) before and (d) after 5000 cycles.

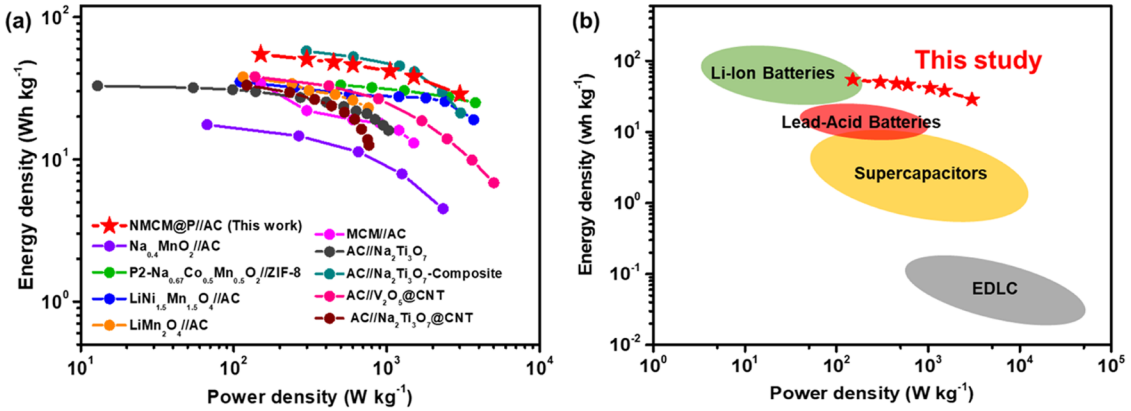

Figure 8. Ragone plot of NMCM@P//AC compared with (a) previously reported SICs and (b) different types of energy storage devices.

and Cu substitution stabilized the structure at a high voltage. Also, a sodium phosphate layer coated by simple melt impregnation was clarified using ToF−SIMS. This layer protected the surface of the active materials from damage while suppressing byproduct formation. As a result, the assembled SIC based on NMCM@P and AC showed better energy density, power density, and cyclic stability than those of other SICs using battery-type cathodes.

■ ASSOCIATED CONTENT

Supporting Information

The Supporting Information is available free of charge at https://pubs.acs.org/doi/10.1021/acsami.3c13351.

ICP−OES result of NMCM, results of ToF-SIMS, FT-IR, and Raman spectroscopy of NMCM and NMCM@P, SEM and TEM images, and CV profiles of NMCM and NMCM@P; charge−discharge curves, rate capability, and cyclic stability of AC, NM, NMM, NMC, NMCM, and NMCM@P. SIC charge−discharge curves with different N/P ratios; CV curves of NMCM//AC SICs; cycle stability evaluation according to coating amount (PDF)

■ AUTHOR INFORMATION

Corresponding Authors

Yun-Sung Lee − *School of Chemical Engineering, Chonnam National University, Gwangju 61186, Republic of Korea;* orcid.org/0000-0002-6676-2871; Email: Email: leeys@chonnam.ac.kr

Yong Il Park − *School of Chemical Engineering, Chonnam National University, Gwangju 61186, Republic of Korea;* orcid.org/0000-0003-3167-4908; Email: ypark@jnu.ac.kr

https://doi.org/10.1021/acsami.3c13351
ACS Appl. Mater. Interfaces 2023, 15, 54530−54538

Authors

Song Yeul Lee − *School of Chemical Engineering, Chonnam National University, Gwangju 61186, Republic of Korea*

Yang Soo Kim − *Korea Basic Science Institute, Jeonju 54907, Republic of Korea*

Sangho Park − *Department of Battery Engineering, Dongshin University, Naju 58245, Republic of Korea*

Complete contact information is available at: https://pubs.acs.org/10.1021/acsami.3c13351

Notes

The authors declare no competing financial interest.

■ ACKNOWLEDGMENTS

This work was supported by the National Research Foundation of Korea (NRF) grant funded by the Korea government (Ministry of Science, ICT & Future Planning) (Nos. 2019R1A4A2001527 and 2021R1I1A3047374). This work was also supported by the Korea Basic Science Institute (Grant No. C210200).

■ REFERENCES

(1) Gogotsi, Y.; Simon, P. True Performance Metrics in Electrochemical Energy Storage. *Science* **2011**, *334*, 917−918.

(2) Dunn, B.; Kamath, H.; Tarascon, J.-M. Electrical Energy Storage for the Grid: a Battery of Choices. *Science* **2011**, *334*, 928−935.

(3) Bruce, P. G.; Freunberger, S. A.; Hardwick, L. J.; Tarascon, J.-M. Li−O_2 and Li−S Batteries with High Energy Storage. *Nat. Mater.* **2012**, *11*, 19−29.

(4) Tarascon, J.-M. Is Lithium the New Gold? *Nat. Chem.* **2010**, *2*, 510.

(5) Kang, K.; Meng, Y. S.; Bréger, J.; Grey, C. P.; Ceder, G. Electrodes with High Power and High Capacity for Rechargeable Lithium Batteries. *Science* **2006**, *311*, 977−980.

(6) Lim, E.; Chun, J.; Jo, C.; Hwang, J. Recent Advances in the Synthesis of Mesoporous Materials and Their Application to Lithium-Ion Batteries and Hybrid Supercapacitors. *Korean J. Chem. Eng.* **2021**, *38*, 227−247.

(7) Yabuuchi, N.; Kubota, K.; Dahbi, M.; Komaba, S. Research Development on Sodium-Ion Batteries. *Chem. Rev.* **2014**, *114*, 11636−11682.

(8) Fang, Y.; Xiao, L.; Chen, Z.; Ai, X.; Cao, Y.; Yang, H. Recent Advances in Sodium-Ion Battery Materials. *Electrochem. Energy Rev.* **2018**, *1*, 294−323.

(9) Kumar, R.; Joanni, E.; Sahoo, S.; Shim, J.-J.; Tan, W. K.; Matsuda, A.; Singh, R. K. An Overview of Recent Progress in Nanostructured Carbon-Based Supercapacitor Electrodes: from Zero to Bi-Dimensional Materials. *Carbon* **2022**, *193*, 298−338.

(10) Mohammed, L.; Boating, B.; Mwemezi, M.; Hamenu, L.; Madzvamuse, A.; Nyarko, A.; Mohammed, M.; Oduro, W.; Agyenim, F. B.; Lee, Y. M.; Ko, J. M. EMI-BF_4 Electrolyte and Al_2O_3/PVDF-HFP Modified PE Separator for High Capacitance Retention and Cycle Stability in Supercapacitors. *Korean J. Chem. Eng.* **2022**, *39*, 3003−3011.

(11) Xiao, X.; Duan, X.; Song, Z.; Deng, X.; Deng, W.; Hou, H.; Zheng, R.; Zou, G.; Ji, X. High-Throughput Production of Cheap Mineral-Based Heterostructures for High Power Sodium Ion Capacitors. *Adv. Funct. Mater.* **2022**, *32*, No. 2110476.

(12) Zuo, W.; Li, R.; Zhou, C.; Li, Y.; Xia, J.; Liu, J. Battery-Supercapacitor Hybrid Devices: Recent Progress and Future Prospects. *Adv. Sci.* **2017**, *4*, No. 1600539.

(13) Wang, X.; Kajiyama, S.; Iinuma, H.; Hosono, E.; Oro, S.; Moriguchi, I.; Okubo, M.; Yamada, A. Pseudocapacitance of MXene Nanosheets for High-Power Sodium-Ion Hybrid Capacitors. *Nat. Commun.* **2015**, *6*, No. 6544.

(14) Glushenkov, A. M.; Ellis, A. V. Cell Configurations and Electrode Materials for Nonaqueous Sodium-Ion Capacitors: the Current State of the Field. *Adv. Sustainable Syst.* **2018**, *2*, No. 1800006.

(15) Huang, Z.-X.; Gu, Z.-Y.; Heng, Y.-L.; Huixiang Ang, E.; Geng, H.-B.; Wu, X.-L. Advanced Layered Oxide Cathodes for Sodium/Potassium-Ion Batteries: Development, Challenges and Prospects. *Chem. Eng. J.* **2023**, *452*, No. 139438.

(16) Wang, D.; Deng, Y.-P.; Liu, Y.; Jiang, Y.; Zhong, B.; Wu, Z.; Guo, X.; Chen, Z. Sodium-Ion Batteries towards Practical Application through Gradient Mn-Based Layer-Tunnel Cathode. *Nano Energy* **2023**, *110*, No. 108340.

(17) Wang, P.-F.; You, Y.; Yin, Y.-X.; Wang, Y.-S.; Wan, L.-J.; Gu, L.; Guo, Y.-G. Suppressing the P2−O2 Phase Transition of $Na_{0.67}Mn_{0.67}Ni_{0.33}O_2$ by Magnesium Substitution for Improved Sodium-Ion Batteries. *Angew. Chem., Int. Ed.* **2016**, *55*, 7445−7449.

(18) Ma, C.; Alvarado, J.; Xu, J.; Clément, R. J.; Kodur, M.; Tong, W.; Grey, C. P.; Meng, Y. S. Exploring Oxygen Activity in the High Energy P2-Type $Na_{0.78}Ni_{0.23}Mn_{0.69}O_2$ Cathode Material for Na-Ion Batteries. *J. Am. Chem. Soc.* **2017**, *139*, 4835−4845.

(19) Singh, G.; Tapia-Ruiz, N.; Lopez del Amo, J. M.; Maitra, U.; Somerville, J. W.; Armstrong, A. R.; Martinez de Ilarduya, J.; Rojo, T.; Bruce, P. G. High Voltage Mg-Doped $Na_{0.67}Ni_{0.3-x}Mg_xMn_{0.7}O_2$ (x = 0.05, 0.1) Na-Ion Cathodes with Enhanced Stability and Rate Capability. *Chem. Mater.* **2016**, *28*, 5087−5094.

(20) Hou, H.; Gan, B.; Gong, Y.; Chen, N.; Sun, C. P2-type $Na_{0.67}Ni_{0.23}Mg_{0.1}Mn_{0.67}O_2$ as a High-Performance Cathode for a Sodium-Ion Battery. *Inorg. Chem.* **2016**, *55*, 9033−9037.

(21) Kang, W.; Zhang, Z.; Lee, P.-K.; Ng, T.-W.; Li, W.; Tang, Y.; Zhang, W.; Lee, C.-S.; Wai Yu, D. Y. Copper Substituted P2-Type $Na_{0.67}Cu_xMn_{1-x}O_2$: a Stable High-Power Sodium-Ion Battery Cathode. *J. Mater. Chem. A* **2015**, *3*, 22846−22852.

(22) Alvarado, J.; Ma, C.; Wang, S.; Nguyen, K.; Kodur, M.; Meng, Y. S. Improvement of the Cathode Electrolyte Interphase on P2-$Na_{2/3}Ni_{1/3}Mn_{2/3}O_2$ by Atomic Layer Deposition. *ACS Appl. Mater. Interfaces* **2017**, *9*, 26518−26530.

(23) Ramasamy, H. V.; Kaliyappan, K.; Thangavel, R.; Aravindan, V.; Kang, K.; Kim, D. U.; Park, Y.; Sun, X.; Lee, Y.-S. Cu-Doped P2-$Na_{0.5}Ni_{0.33}Mn_{0.67}O_2$ Encapsulated with MgO as a Novel High Voltage Cathode with Enhanced Na-Storage Properties. *J. Mater. Chem. A* **2017**, *5*, 8408−8415.

(24) Lamb, J.; Manthiram, A. Surface-Modified $Na(Ni_{0.3}Fe_{0.4}Mn_{0.3})O_2$ Cathodes with Enhanced Cycle Life and Air Stability for Sodium-Ion Batteries. *ACS Appl. Energy Mater.* **2021**, *4*, 11735−11742.

(25) Abdel-Kader, A.; Ammar, A. A.; Saleh, S. I. Thermal Behaviour of Ammonium Dihydrogen Phosphate Crystals in the Temperature Range 25−600° C. *Thermochim. Acta* **1991**, *176*, 293−304.

(26) Li, W.; Yao, Z.; Zhang, S.; Wang, X.; Xia, X.; Gu, C.; Tu, J. Building Superior Layered Oxide Cathode via Rational Surface Engineering for Both Liquid & Solid-State Sodium Ion Batteries. *Chem. Eng. J.* **2021**, *421*, No. 127788.

(27) Lee, D. H.; Xu, J.; Meng, Y. S. An Advanced Cathode for Na-Ion Batteries with High Rate and Excellent Structural Stability. *Phys. Chem. Chem. Phys.* **2013**, *15*, 3304−3312.

(28) Lu, Z.; Dahn, J. R. In Situ X-ray Diffraction Study of P2$Na_{2/3}[Ni_{1/3}Mn_{2/3}]O_2$. *J. Electrochem. Soc.* **2001**, *148*, A1225.

(29) Moeez, I.; Susanto, D.; Chang, W.; Lim, H.-D.; Chung, K. Y. Artificial Cathode Electrolyte Interphase by Functional Additives toward Long-Life Sodium-Ion Batteries. *Chem. Eng. J.* **2021**, *425*, No. 130547.

(30) Jiao, S.; Ren, X.; Cao, R.; Engelhard, M. H.; Liu, Y.; Hu, D.; Mei, D.; Zheng, J.; Zhao, W.; Li, Q.; et al. Stable Cycling of High-Voltage Lithium Metal Batteries in Ether Electrolytes. *Nat. Energy* **2018**, *3* (9), 739−746.

(31) Gu, H.; Kong, L.; Cui, H.; Zhou, X.; Xie, Z.; Zhou, Z. Fabricating High-Performance Sodium Ion Capacitors with P2-$Na_{0.67}Co_{0.5}Mn_{0.5}O_2$ and MOF-Derived Carbon. *J. Energy Chem.* **2019**, *28*, 79−84.

(32) Wasiński, K.; Półrolniczak, P.; Walkowiak, M. Proof-of-Concept Study of a New Type Sodium-Ion Hybrid Electrochemical Capacitor with Organic Electrolyte. *Electrochim. Acta* **2018**, *259*, 850−854.
(33) Li, H.; Cheng, L.; Xia, Y. A Hybrid Electrochemical Supercapacitor Based on a 5 V Li-Ion Battery Cathode and Active Carbon. *Electrochem. Solid-State Lett.* **2005**, *8*, A433.
(34) Kwon, Y. K.; Choi, W.; Choi, H.-S.; Lee, J. K. Effect of Lithium Difluoro(oxalato)borate on $LiMn_2O_4$-Activated Carbon Hybrid Capacitors. *Electron. Mater. Lett.* **2013**, *9*, 751−754.
(35) Kim, H.-J.; Ramasamy, H. V.; Jeong, G.-H.; Aravindan, V.; Lee, Y.-S. Deciphering the Structure−Property Relationship of Na−Mn−Co−Mg−O as a Novel High-Capacity Layered−Tunnel Hybrid Cathode and Its Application in Sodium-Ion Capacitors. *ACS Appl. Mater. Interfaces* **2020**, *12*, 10268−10279.
(36) Dong, S.; Shen, L.; Li, H.; Nie, P.; Zhu, Y.; Sheng, Q.; Zhang, X. Pseudocapacitive Behaviours of $Na_2Ti_3O_7$@CNT Coaxial Nanocables for High-Performance Sodium-Ion Capacitors. *J. Mater. Chem. A* **2015**, *3* (42), 21277−21283.
(37) Yin, J.; Qi, L.; Wang, H. Sodium Titanate Nanotubes as Negative Electrode Materials for Sodium-Ion Capacitors. *ACS Appl. Mater. Interfaces* **2012**, *4* (5), 2762−2768.
(38) Zhao, L.; Qi, L.; Wang, H. Sodium Titanate Nanotube/Graphite, an Electric Energy Storage Device Using Na^+-Based Organic Electrolytes. *J. Power Sources* **2013**, *242*, 597−603.
(39) Chen, Z.; Augustyn, V.; Jia, X.; Xiao, Q.; Dunn, B.; Lu, Y. High-Performance Sodium-Ion Pseudocapacitors Based on Hierarchically Porous Nanowire Composites. *ACS Nano* **2012**, *6* (5), 4319−4327.

https://doi.org/10.1021/acsami.3c13351
ACS Appl. Mater. Interfaces 2023, 15, 54530−54538